Technische Universität München
Fakultät für Physik

Abschlussarbeit im Bachelorstudiengang Physik

Cryogenic packaging in silicon nanophotonics

Ria Maria Anita Rosenauer

August 29th 2022

Durchgeführt in der Otto-Hahn-Gruppe "Quantennetzwerke" am Max-Planck-Institut für Quantenoptik

Erstgutachter (Themensteller): Prof. Dr. A. Reiserer
Zweitgutachter: Prof. Dr. P. Müller-Buschbaum

Contents

Abstract

In today's information technology infrastructure, photons in optical glass fibers are used to send information over long distances at high rates of transmission. Upon arrival, the information encoded in the photons can be extracted in on-chip devices, so called photonic integrated circuits (PICs). This combination of photons in fibers and PICs offers many advantages, however one of the major problems is the size-mismatch between waveguide modes in PICs and in optical glass fibers requiring sophisticated fiber-to-chip coupling techniques in order to avoid losses at the fiber-to-chip interface. Additionally, when coupling is performed at cryogenic temperatures below 2 K, which is the case for many experiments that involve quantum systems, a compromise between robustness, ease of fabrication, broadband transmission and efficiency needs to be found. This is the challenge of cryogenic packaging. A widely used fiber-to-chip coupling technique is adiabatic coupling, which offers several advantages like easy fabrication, broadband functionality and robustness at cryogenic temperatures. However, the coupling efficiency strongly depends on the chips' and PICs' properties. In their recent publication, Khan et al. present a novel approach for increasing the coupling efficiency of adiabatic coupling by using tapered fibers where the fiber tips are coated with a photoresist [1]. The authors describe coupling efficiencies of over 90% by using these capped fibers for coupling into silicon nitride waveguides. The aim of this thesis is to investigate if the results and techniques reported in [1] can be adapted to adiabatic coupling into silicon ridge waveguides. First, I report on numerical simulations modeling the adiabatic coupling technique and then I go on to describe my work on fabricating the capped tapered fibers as well as some first characterization measurements.

Chapter 1

Introduction

One of the most important applications of Maxwell's equations today is the transmission and processing of information. Typically, the information handling takes place in devices, where the processing is done via electronics using electrons in integrated circuits. Often, information used in electronic devices is exchanged between them via photons in optical glass fibers, as this allows for high transmission rates and low loss of information even at large distances. Thus, in large networks, like the internet, the transmission signal is entirely composed of photons, where information can be encoded in intensity, polarization or wavelength of light. In order to generate, read and manipulate electromagnetic signals in general, very large free-space setups with lenses, mirrors and other optical components were required in earlier days. While those components are typically available in a well-equipped laboratory, for practical purposes and for up-scaling other solutions are needed [2].

In order to overcome this need for highly sophisticated free-space setups, in the last decades, the new field of integrated photonics has emerged. In integrated photonics, light is manipulated and distributed on a chip, using so-called photonic integrated circuits (PICs). These PICs have several advantages: They typically do not suffer from electromagnetic interference, they feature small sizes and small weight and show improved reliability to only name a few [3]. Over time, the components on the PICs became smaller and smaller resulting in configurations where the size of the components are on the same order of magnitude or even smaller than the wavelength of light used in these structures. At these length scales, optical ray methods fail to adequately describe the relevant physics, thus one typically uses wave optics instead. The research field describing photonic structures at these length scales is called nanophotonics. It does not only allow for the design of even smaller PICs, it also is able to predict and explain a whole new plethora of physical phenomena such as plasmonics, nanophotonic crystals and metamaterials [4–6]. In many cases, a PIC uses waveguides to guide the light on the chip. The additional components using or manipulating the light on the chip depend on the targeted application. Example components are nanometer-scale mirrors, optical cavities or even on-chip modulators [7–9]. The use of erbium ions as emitters embedded in silicon is investigated in the "Quantum Networks group" at the Max Planck Institute of Quantum Optics. Here, the goal is to realize a scalable quantum network, enabling transmission of quantum information between spatially separated quantum systems. This platform is highly promising for applications in a future quantum network, as it combines the good optical properties of erbium ions and the mature and well-developed silicon nanophotonic platform. The realization of such a network would tackle the scalability problems in nanophotonics in different areas, such as quantum computing, communication and sensing [10–12]. A major challenge for achieving this goal is the realization of a deterministic way to distribute entanglement in such a network. For that, memories used in so called quantum repeaters play an important role [13]. A promising approach for such kind of memories is the implantation of

erbium ions into silicon waveguides in nanophotonic PICs [14, 15]. A sketch of a typical erbium-doped waveguide used in this approach is shown in Figure 1.1. As erbium emits light at $\lambda \approx 1536\,\text{nm}$, the refractive indices given in this thesis are given as $n(\lambda = 1536\,\text{nm})$.

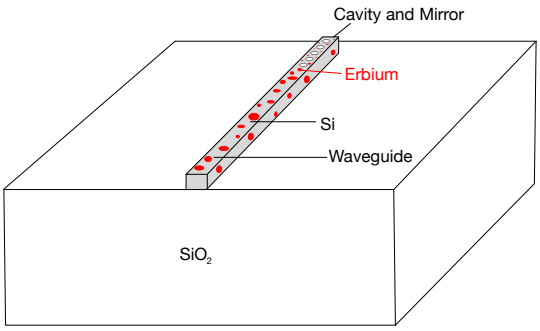

Figure 1.1: **Sketch of an example PIC**
The PIC shown here is a typical example for a PIC used by the "Quantum Networks group" for implementing a quantum memory network node. An erbium-doped silicon waveguide with rectangular cross-section resides on top of a silicon dioxide buried oxide layer. Light is coupled into the waveguide at the front and is then confined in the waveguide by total internal reflection. The waveguide is terminated with a broadband photonic crystal mirror, which reflects light back towards the waveguides front facet.

Typically, the length of on-chip waveguides is on the order of several hundred nanometers. The goal now is to efficiently couple light into these waveguides. For transmitting light over large distances, an optical glass fiber is often used since it is cheap, robust and easy to handle. Unfortunately, there is a large size-mismatch between the cross-section of a nanophotonic waveguide (e.g. $220\,\text{nm} \times 700\,\text{nm}$) and a typical optical glass fiber featuring a mode diameter of around $8\,\mu\text{m}$. Therefore, establishing a deterministic *fiber-to-chip coupling*, i.e. to reliably transmit signals from optical fibers into those small waveguide structures, is a challenge. For the experiments done in the "Quantum Networks Group" there is an additional problem: The coupling often has to take place in cryostats, as the spectroscopy experiments performed on the chip require extremely low temperatures on the order of $2\,\text{K}$. This means that not only a high coupling efficiency is needed, but the coupling technique needs to be robust enough to still work at cryogenic temperatures. The area of research that deals with the robust coupling is called *cryogenic packaging* and is dedicated to the optimization of interfacing PICs at low temperatures. Over the last few years, a lot of different coupling solutions were introduced [16], which will be reviewed in detail later in this thesis.

The work described here presents a specific coupling approach that increases the coupling efficiency of a tapered optical fiber into a silicon waveguide. It is based on the paper *"Low-loss, high-bandwidth fiber-to-chip coupling using capped adiabatic tapered fibers"* [1], where a new approach using SU8 capped tapered fibers for efficient fiber-to-chip coupling is investigated. Instead of the silicon waveguides used by the "Quantum Networks Group", the authors of [1] use waveguides made out of silicon nitride (SiN). This thesis investigates if their approach is applicable to our case despite the large difference in the refractive index of

silicon ($n_{Si} = 3.5$) and silicon nitride ($n_{SiN} = 2.0$), by first simulating this specific coupling idea with silicon waveguides, to estimate the theoretically achievable coupling efficiencies. Then, a recipe to replicate the coating process of tapered fibers with SU8 described in [1] is developed. The coupling performance of the coated fibers is investigated experimentally. Additionally, the experimental setups and the fabrication of the capped tapered fibers are explained in detail. Finally, this thesis also reports on simulations evaluating the use of SU8 coating enabling the gluing of tapered fibers onto waveguides.

Chapter 2

Theoretical Background

As described in the introduction, the goal of this thesis is to investigate a specific fiber-to-chip coupling approach for adiabatic coupling with tapered fibers. Therefore, I will describe how adiabatic coupling with tapered fibers works from a theoretical point of view. To do that one first has to understand what optical modes are and how they are involved in guiding light in the waveguides relevant for this thesis (on-chip ridge waveguide and optical fiber). Afterwards, an introduction to adiabatic coupling with tapered fibers is given. For the investigation of novel coupling approaches I present numerical simulations describing the complex nanophotonic coupling approach and review the FDTD technique used for this kind of simulations.

2.1 Optical waveguides

Fiber-to-chip coupling is relevant in all fields where light has to be transmitted over large distances and is then processed on the chip. An ideal tool for distributing the light are waveguides. Waveguides used for large distance transmission are usually optical fibers, whereas on-chip guiding of light takes place in smaller waveguides. In this thesis, silicon ridge waveguides are the relevant on-chip waveguides. In the following, I first want to give a general introduction on how to analyze light propagating in waveguides and then have a closer look at the specific examples for the waveguides used in this thesis, namely optical fibers and silicon ridge waveguides.

Waveguides are defined by their geometry and the material they are composed of. Thus, knowledge of the spatial dependence of the refractive index $n(\vec{r})$ is sufficient to predict the propagation of light by solving Maxwell's equations. The analysis of waveguides consists of finding the solutions to Maxwell's equations that satisfy the boundary conditions imposed by the geometry of the waveguide. The fundamental solutions that form the basis for all possible solutions are then called *modes* [17, 18]. For waveguides guiding light in a single fixed direction, without loss of generality in $\vec{e}_z$ direction, one can show using Maxwell's curl equations that it is sufficient to calculate the E_z and H_z component of an electromagnetic wave and the other components automatically follow [19]. As there are no boundary conditions in z-direction, the form of the possible electromagnetic waves is assumed to be

$$\vec{E}(x,y,z) = \vec{f}_E(x,y)e^{-i(\omega t-\beta z)} \tag{2.1}$$

$$\vec{B}(x,y,z) = \vec{f}_B(x,y)e^{-i(\omega t-\beta z)} \tag{2.2}$$

where $\vec{f}(x,y)$ is is the vector amplitude of the $\vec{E}$/ $\vec{B}$-fields that is translationally invariant in z-direction, $\omega = 2\pi f$ the angular frequency and β the propagation constant of the electromagnetic wave in the respective material. With this, the propagation properties of light within a homogeneous, isotropic waveguide with material constants μ and ϵ can be

calculated by solving the Helmholtz equation

$$\nabla^2 \begin{bmatrix} H_z \\ E_z \end{bmatrix} = -(\omega^2 \mu\epsilon - \beta^2) \begin{bmatrix} H_z \\ E_z \end{bmatrix} \tag{2.3}$$

The detailed derivation of equation 2.3 can be found for example in [17]. The simplest examples of solutions to the Helmholtz equation are found in a homogeneous, isotropic medium, where the modes are plane waves of the form $\vec{E_0} e^{i(\vec{k}\vec{r}-\omega t)}$, $\omega = \frac{c}{n}|\vec{k}|$ with $n = \sqrt{\mu\epsilon}$. Any signal in free-space can be decomposed into a linear superposition of such waves. In materials that are not homogeneous the solutions for equation 2.3 are more complicated. Two important modes used in this thesis, the modes in silicon ridge waveguides and optical glass fibers are discussed in the following.

2.1.1 Silicon ridge waveguides

The on-chip waveguides relevant for this thesis are called ridge waveguides. In our case they consist of a strip of silicon with refractive index $n = 3.5$ on top of a low-index layer called buried oxide (BOx) that consists of SiO_2 with $n = 1.45$. Due to the refractive index contrast, the light is confined in the silicon strip by total internal reflection. The outline of such a ridge waveguide with the geometry relevant for this thesis can be seen in Figure 2.1. The shown waveguide guides three modes, two transverse electric (TE) modes and one transverse magnetic mode. The shown fundamental mode profile was simulated with an open-source software called MPB [20], which is a frequency-domain eigensolver. An analysis of the allowed mathematical solutions for the guiding modes in such a waveguide can be found in [21].

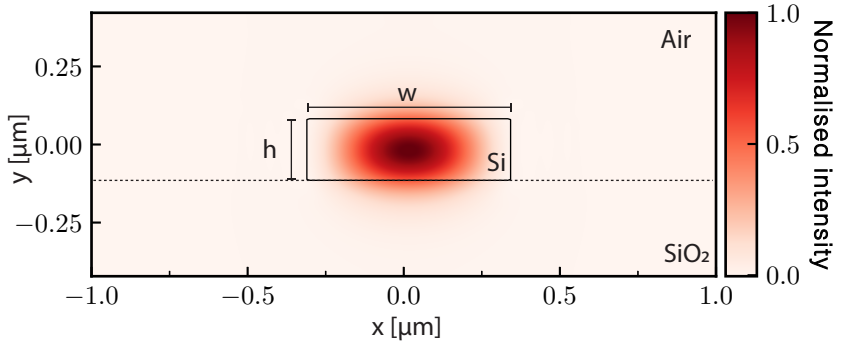

Figure 2.1: **Geometry and mode profile of a ridge waveguide**
The shown cross-section depicts the geometry relevant for the silicon waveguides described in this thesis. A silicon strip of height $h = 220\,\text{nm}$ and width $w = 700\,\text{nm}$ with $n = 3.5$ resides on top of a buried oxide layer (SiO_2) of height $w_2 = 3\,\mu\text{m}$ with $n = 1.45$. The plotted intensity visualizes the mode profile of the guided fundamental mode. Figure adapted from [22]

.

2.1.2 Optical glass fibers

The previous section described waveguides that confine light on a silicon chip. The waveguides used to transmit signals over larger distances are usually optical fibers. There exists a huge variety of optical fibers for a broad range of applications. Examples include single-mode fibers used for long distance communication, multi-mode graded index fibers, rather used for short range communication and multi-mode step index fibers which are

suited for applications requiring high power densities [23].

For this thesis only commercially available single-mode (SMF) step-index fibers are relevant. A sketch of the widely used SMF-28 fibers can be seen in Figure 2.2. The refractive index in cylindrical coordinates (ρ, θ, z) is given as

$$n(\rho, \theta, z) = \begin{cases} n_{co} & 0 \leq \rho \leq r_{co} \\ n_{cl} & r_{co} < \rho \leq r_{cl} \\ n_{sur} & r_{cl} < \rho \end{cases} \tag{2.4}$$

The region $0 < r < r_{co}$ is called core, $r_{co} < r < r_{cl}$ is called cladding and $r_{cl} < r$ is the surrounding. Here, n_{co}, n_{cl}, n_{sur} are the refractive indices of core, cladding and surrounding and r_{co}, r_{cl} are the radii of core and cladding. For SMF-28 fibers it holds that $n_{co} = 1.462$, $r_{co} = 8.2\,\mu\text{m}$, $n_{cl} = 1.457$ and $r_{cl} = 125\,\mu\text{m}$ [24].

The modes of the step index fibers can be classified into three types of modes [18]:

- core modes
- cladding modes
- radiation modes

The underlying mathematical classification derived from the types of solutions to one differential equation that determines the radial and azimuthal dependence of the $\vec{E}$ and $\vec{H}$ fields. To be more specific, the difference between this solution types is, in which region (core or cladding) they are well-defined and physical (e.g. do not diverge and decay sufficiently fast for $r \to \infty$) [25, 26]. The core modes for optical fibers are called linearly polarized (LP) modes. The modes LP_{nm} are indexed by the non-negative integers n and m, which are parameters determining the geometry of the solution. A detailed listing of the mathematical formula for each LP_{nm} mode can be found in [27]. The fundamental mode of glass fibers is given by the LP_{01} mode, which is also depicted in Figure 2.2.

As the name suggests, single-mode fibers guide only a single-mode, the so called fundamental mode. The conditions that have to be satisfied for a fiber to be a single-mode fiber are specified by the dimensionless effective index V:

$$V = \frac{2\pi r_{co}}{\lambda} \sqrt{n_{co}^2 - n_{cl}^2} < 2.405 \tag{2.5}$$

Here λ is the wavelength of the light propagating through the fiber. A derivation of equation 2.5 can be found in [26].

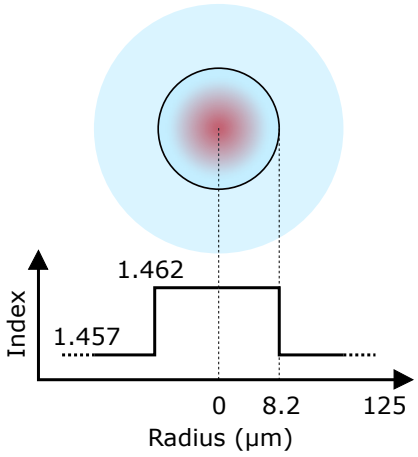

Figure 2.2: **Structure and refractive index of SMF-28 fibers**
SMF-28 fibers are single-mode optical fibers used for transmitting light over large distances. They consist of a core with diameter $r_{co} = 8.2\,\mu m$ made of Germanium-doped fused silica glass with refractive index $n_{co} = 1.462$ and a cladding from undoped fused silica with diameter $r_{cl} = 125\,\mu m$ and refractive index $n_{cl} = 1.457$. The schematic mode field at the center of the core visualises the approximate intensity profile of the fundamental mode (LP_{01}) of the depicted optical fiber.

2.2 Fiber-to-chip coupling

Previously, the two waveguides involved in transmitting and processing electromagnetic waves were introduced. Fiber-to-chip coupling now deals with the problem of coupling laser light from the introduced optical fiber to the on-chip waveguide. This is important for all applications, where an electromagnetic signal has to be sent to or from a PIC. In the previous section it was seen that the geometry, size and materials of fibers and on-chip waveguides are quite different. The resulting differences of fundamental core mode sizes and refractive indices make efficient fiber-to-chip coupling very challenging.

The following paragraph is a brief summary of chapter three from [16], which gives a good overview of different fiber-to-chip coupling techniques. To minimize the problems arising from different refractive indices and fundamental core mode sizes of fiber and on-chip waveguide, one has to ensure that the modes have a maximum overlap in their field (real-space) and momentum (k-space) distribution. This is called mode matching. Mode matching in real space means to design the coupling in a way, that the overlap integral of the fundamental core modes in fiber and waveguide is maximized. If real space matching is poor, the electromagnetic signal will be coupled to cladding and/or radiation modes, which decreases the coupling efficiency. Mode matching in k-space (momentum-space) means that the difference in propagation vector of the different waveguide materials has to be efficiently transformed. Otherwise unwanted scattering and back-reflection will occur. To practically realize a transition of waveguides that satisfy the conditions of efficient coupling, there are four established techniques that can be used: Adiabatic transitions, diffraction-based coupling (via periodic gratings), multi-mode or multi-path interference and resonant coupling. The implementation of these four mechanisms can again be divided into two different types of solution implementations: First there are edge-coupling solutions, where the edge of the incoming fiber is aligned to the propagation axis of the light

in the waveguide. The second type are surface-coupling solutions, where the light from the optical fibers incidents from the surface of the chip [28–30]. For edge couplers, two more types of coupling solutions can be differentiated. First, there are butt couplers, where a cleaved fiber, a fiber with a perfectly flat facet, is brought close to a mode converter and coupled into the waveguide.. Second, tapered fiber coupling exist, where fiber and waveguide are tapered in such a way, that no jump in effective refractive index occurs.

Every coupling method has its pros and cons. Grating couplers, for example, are typically narrow-band, and difficult to fabricate when high efficiencies are targeted [30]. Side couplers are broadband, but require very good alignment and are inefficient without suited mode converters. Previously investigated structures were difficult to fabricate and/or fragile when operated under cryogenic conditions. Adiabatic coupling has the advantage of broadband coupling and ease of fabrication, but at the same time the coupling efficiencies achieved with the current methods are not good enough [16].

2.2.1 Adiabatic coupling with tapered fibers

As described above, adiabatic coupling has several advantages, but so far the realized coupling efficiency needs to be improved. Therefore, the overall goal of the presented work in this thesis is the improvement of adiabatic coupling with tapered fibers. In order to understand these improvement ideas I will take a closer look at specifically this type of coupling in this chapter. An important concept for understanding adiabatic coupling is adiabatic mode transformation. Here, a waveguide guiding light in z-direction is assumed, where the change in the parameters of the waveguide geometry (e.g. change in radius) along the z-direction happens so slowly that the local mode at every z-position can be approximated with an infinitely long waveguide having exactly the index profile at that point [31].

The idea of adiabatic coupling is to have a smooth transition from the mode guided in a nanophotonic waveguide to that in an optical fiber. This is achieved by tapering both the waveguide and the fiber, and bringing them in contact with one another, as can be seen for example in Figure 2.3 (b). Because of the adiabatic mode transformation, during the light transfer from the fundamental mode of the fiber to the waveguide, no coupling to higher order modes or radiation modes is expected. This means that almost all power is transitioned between the two modes in both silicon waveguide and optical fiber [32].

For the adiabatic coupling used in this thesis, silicon waveguides are used. A combination of theoretical and experimental results [33, 32] was used to determine the taper angle for the fiber and the taper geometry of the waveguide. A sketch describing the coupling scheme can be seen in Figure 2.3. The fiber is tapered at a 3° angle. The waveguide is tapered from a width of 0.65 µm down to a width of 0.2 µm over a length of 40 µm.

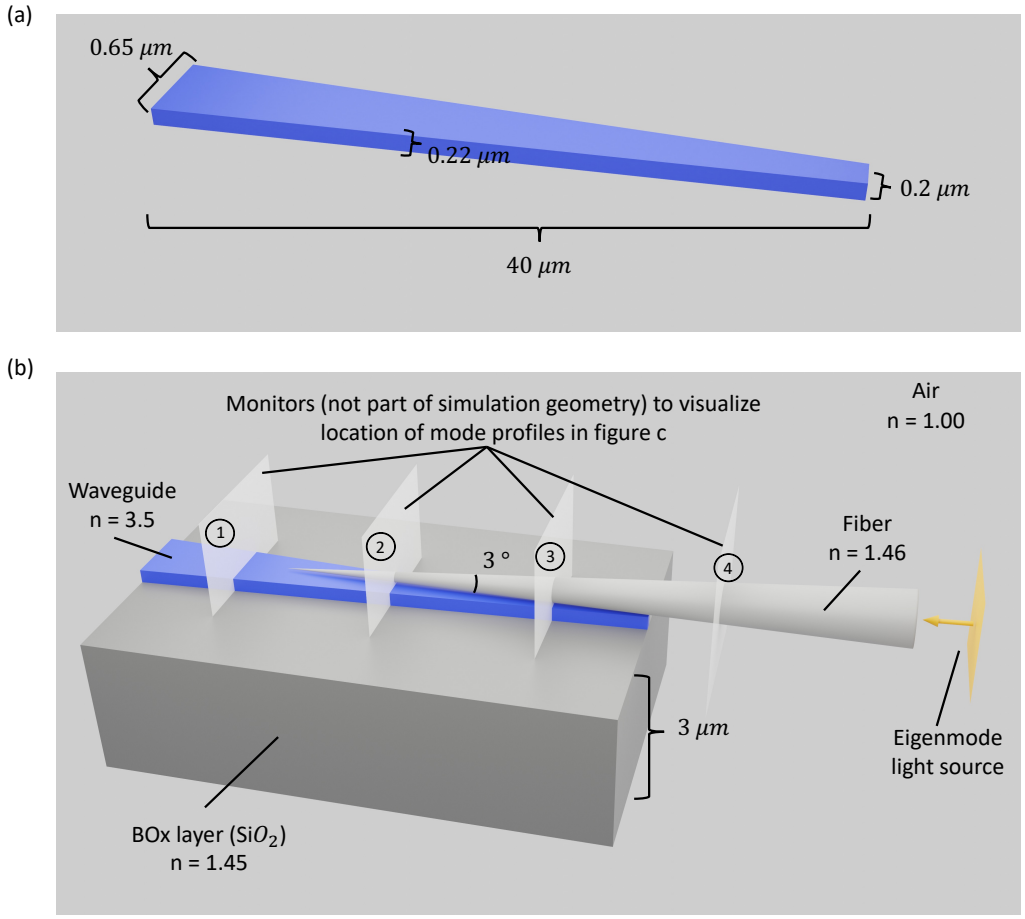

Figure 2.3: **Adiabatic coupling simulation with a tapered fiber**
Figure (a) and (b) depict the implementation of adiabatic coupling between tapered fiber and silicon ridge waveguide used for the simulations in this thesis. An eigenmode light source excites the fundamental fiber mode, which propagates through the tapered fiber and is adiabatically coupled into the tapered silicon waveguide. The four planes drawn are not part of the geometry and only represent the positions of the four intensity profiles shown in Figure (c). In Figure (c) it can be clearly seen how the intensity slowly shifts from inside the fiber (monitor 4) to inside the waveguide (monitor 1).

2.3 Simulation of optical waveguides using the FDTD method

Having introduced the waveguides and coupling that are studied in this thesis, I now want to investigate the numerical tools that are used for their investigation. The simulation methods that are now introduced will be used later to get an idea about how good the results from [1] are adaptable to the the coupling implementation used by the "Quantum Networks group". This will help determining, if coating tapered fibers with SU8 is a good idea or if no coupling improvement is to be expected.

The goal of these techniques of computational electromagnetics is to numerically solve Maxwell's equations. There are numerous algorithms that can be used to this end. They can be roughly categorised into integral and differential equation solvers and into time and frequency domain solvers [34]. For the simulations used in this thesis, the finite-difference time-domain method (FDTD) is used, which is a differential equation solver in the time domain. The idea of this solver is to discretize space and time into a lattice. Using the finite-difference method it can be shown, that the $\vec{H}(t + \frac{\Delta t}{2})$ field can be calculated using only $\vec{H}(t - \frac{\Delta t}{2})$ and $\vec{E}(t)$ [35]. The same applies vice versa for $\vec{E}(t + \frac{\Delta t}{2})$, which implies that from $\vec{H}(t + \frac{\Delta t}{2})$ and $\vec{E}(t)$, $\vec{E}(t + \Delta t)$ can be calculated and so on. This method of calculating $\vec{E}$ and $\vec{H}$ in a future time from already known fields is called leap-frog scheme. The calculation in the spacial domain works analogously, meaning that already known fields at specific times and positions lead to the fields at new positions, using the leap-frog scheme. So with this method the time evolution of $\vec{E}(t)$ and $\vec{H}(t)$ are calculated at every point of the space lattice. In order to get $\vec{E}(\omega)$ and $\vec{H}(\omega)$ from these solutions, a discrete fourier-transformation (DFT) is conducted [36].

FDTD is mainly applied in radio-frequency engineering, microwave engineering and nanophotonics. The main advantages of FDTD include its broadband frequency solutions from a single calculation (using DFT), as it is a time domain solver [34, 22]. Also it is very easy to use and to debug and it will always converge, if set up correctly, which are also very valuable features. Because of these benefits, FDTD is used for the simulations shown later in the thesis. Major drawbacks include long computation times and high computational requirements, especially for narrow frequency bands. A typical simulation time for a 1000 fs simulation of an 105 µm × 7.7 µm × 7.3 µm volume was between 30 min and 4 h depending on the mesh setting. Another difficulty when using FDTD is, that at the end of the physical boundaries of the structure, the numerical methods fails, as the mesh ends. However, there is a good way to deal with that lattice truncation problem: Introducing *perfectly matched layers* (PML) at the physical boundaries, which fully absorb any incoming radiation and thus avoid artifacts caused by back-reflections [37].

The software used for all simulations in this thesis is Lumerical. As it is specialized for photonic simulations it is not only very easy to use, it also comes with specialized photonic solutions, like offering conformal and graded meshings, which reduce computational requirements without decreasing accuracy. This gives it a huge advantage over other simulation software like the open source software MEEP [38] for example, which is limited to a cartesian grid meshing.

Chapter 3

Enhancing Fiber-to-Chip Coupling

This chapter deals with all the necessary theoretical and experimental preconditions needed for thoroughly analyzing how good the coupling improvement methods described in [1] are applicable to the setup used by the "Quantum Networks group". First, the coupling improvement method introduced in [1] is discussed and motivated. Then, the simulation setup used to analyze the coupling approach is explained and all the relevant simulation geometries are shown. As this thesis attempts to experimentally verify the simulation results, the experimental setups used for analyzing the coupling improvement method are described, namely the tapered fiber fabrication method, the SU8 coating setup and the optical coupling setup.

3.1 Improvement of the coupling to nanophotonic structures using SU8 capped tapered fibers

In the context of cryogenic packaging, there are several coupling metrics to be considered when searching for the best coupling approach: Robustness, ease of fabrication, broadband transmission and efficiency. The achievable coupling efficiencies with adiabatic coupling strongly depend on the exact implementation and used materials. Adiabatic coupling with tapered fibers can achieve efficiencies of 10% to 20%, when coupling to silicon nanophotonic waveguides residing on a buried oxide layer [22] as shown in Figure 2.3. This method represents a good compromise between broadband transmission, robustness and ease of fabrication. The main drawback using this technique is, that due to the similarity of refractive indices of fiber and BOx, a large part of light coming from the side of the fiber is lost to the continuous modes in the BOx layer [1], leading to a maximum achievable coupling efficiency of around 20% [22]. In the experimental setups used in the "Quantum Networks group" the actual coupling efficiencies are in the range of 10% to 15%, so there is a large room for improvement. A possible approach to solve the efficiency problem of the implementation depicted in Figure 2.3, is to remove the BOx layer underneath the waveguide tip [39] (see Figure 3.1 (a)). Then the coupling takes place in air or vacuum. This can significantly increase coupling efficiencies. Researchers, using for example SiN waveguides [40] or diamond waveguides [41] were able to achieve coupling efficiencies over 90% with that adiabatic coupling technique. The problem with this improvement method however is, that it is difficult to fabricate and very mechanically unstable.

For this reason, Kahn et al. [1] suggest a different solution, namely to coat the tapered fiber with a higher index material as can be seen in 3.1 (b). The idea is, that the coating increases the refractive index difference between the BOx layer and fiber, leading to fewer losses into the BOx layer. In the coupling setup described in [1] a SiN waveguide is used with $n_{SiN} = 2.0$. The authors use an SU8 coating, which is a negative photoresist, having a refractive index of $n_{SU8} = 1.55$ after being developed. Therefore,

$n_{fiber} = 1.46 < n_{SU8} = 1.55 < n_{SiN} = 2.0$, so the light is first coupled from the fiber into the coating and then, because of $n_{SU8} = 1.55 > n_{BOx} = 1.45$ the light is coupled into the silicon nitride waveguide and not into the BOx layer anymore. Because of this mechanism, the authors of [1] describe achieving theoretical coupling efficiencies of more than 90% and experimental efficiencies above 60%.

In this thesis, instead of a SiN waveguide a silicon waveguide is investigated. The reasoning from above is still true as $n_{fiber} = 1.46 < n_{SU8} = 1.55 < n_{Si} = 3.5$ and therefore less light should be lost to the BOx layer. However, the refractive index difference between n_{SU8} and n_{Si} is a lot larger than the difference between n_{SU8} and n_{SiN}. The effects of this index difference are studied in chapter 4.1. The question, why using SU8 and not an even higher refractive index material that is closer to n_{Si} may arise. The answer is, that the coating mechanism described in [1] is very fast, easy and not very expensive, as photoresists have the nice property of being a liquid first, making coating the fiber very easy, as compared to other coating methods like for example sputtering. This would make it worth it even for small coupling improvements.

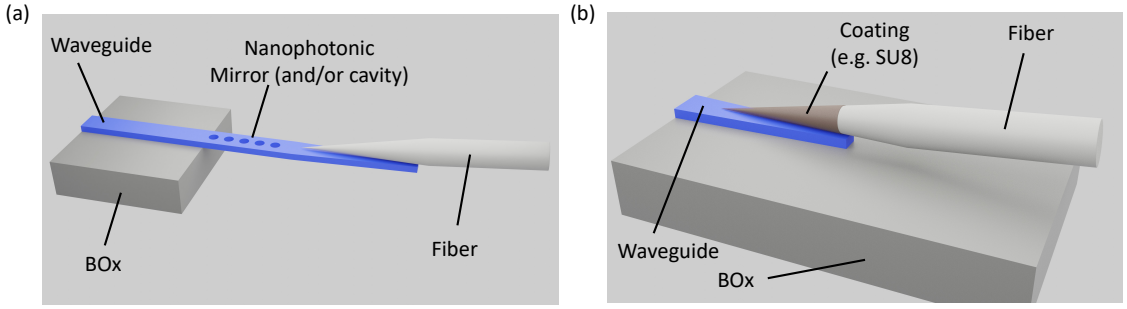

Figure 3.1: **Enhancement of adiabatic coupling with tapered fibers and silicon waveguides on BOx layer**
Figure (a) depicts the idea of etching away the BOx layer below the waveguide, leading to significant coupling efficiency improvements. The implementation shown here etches away the BOx even under on-chip nanophotonic structures such as nanophotonic mirrors and cavities. Figure (b) shows the idea attempted in this thesis, where the tapered fiber is coated with SU8, which has a higher refractive index than the fiber, leading to fewer losses into the BOx layer. Both improvement suggestions are based on the idea of limiting the coupling of the fundamental core fiber mode to the continuum modes in the BOx layer.

3.2 Simulation geometry and sweep parameters for estimating coupling efficiency

In order to simulate the coupling efficiency change of coating tapered fibers with SU8 on the fiber-to-chip coupling setup used by the "Quantum Networks group", the simulation software Lumerical [38] is used, with an FDTD solver as described in 2.3. The geometry of fiber, waveguide and BOx layer used for the following simulations can be found in Figure 2.3 (b) and (c). A source excites an eigenmode Gaussian wave package with wavelength λ between 1500 nm and 1600 nm into the fiber in the direction of the on-chip waveguide. The light propagates along in the fiber towards its tapered tip and then subsequently couples into the silicon waveguide. For the simulations shown here the coating is assumed

to have a conical form, with a slightly smaller angle $\theta < 3°$ than the fiber, so that it slowly thins out and does not end abruptly as would be the case with $\theta = 3°$. A cross-sectional view of the geometry used for coupling can be seen in 3.2. The Figure also shows the parameters that are varied in order to obtain the best parameters for coupling. The thickness of the SU8 coating is influenced by the angle θ and the offset o between the fiber and the coating cone, so sweeping this two parameters helps estimating the theoretical optimal coating thickness. Another parameter that is important for coupling is the overlap length l, describing the length over which the tapered fiber and the waveguide are in contact. This parameter is also investigated for coupling using SU8 coated fiber tips.

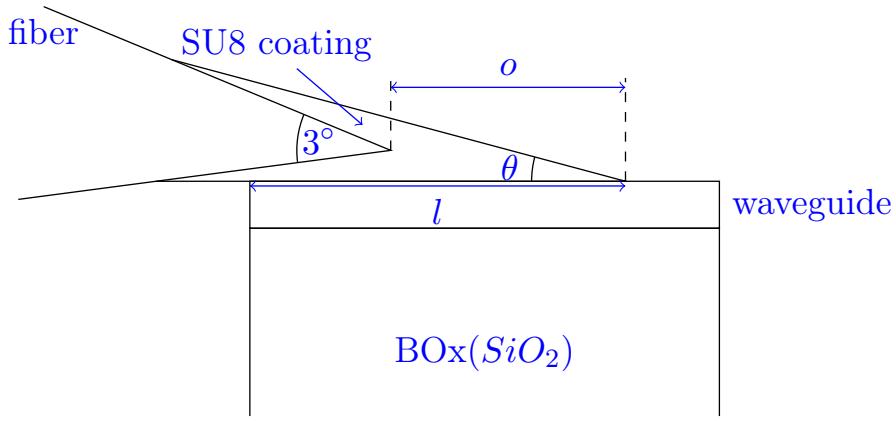

Figure 3.2: **Simulation geometry for capped fiber**
Sketch of the geometry used for the capped fiber simulations. The SU8 coating is modeled as a cone with a slightly smaller angle θ than the angle of 3° of the fiber taper. The set of parameters that are varied to get the optimal coupling are the overlap length l, the offset o between coating tip and fiber tip and the angle θ of the coating.

3.3 Fabrication of tapered fibers

For experimentally verifying the results obtained from the simulations described above, tapered fibers and silicon waveguides on a BOx layer are needed. The fabrication procedure of the PICs with the silicon waveguides are beyond the scope of this thesis. However, as tapered fibers are important for the introduced coupling improvement method with SU8 coating, the fabrication of tapered fibers is shortly summarized in the following. The fabrication procedure is based on the method described in [42]. A batch of standard single-mode SMF-28 fibers is dipped in concentrated hydrofluoric acid (HF). The acid dissolves the SiO_2. By slowly pumping out the HF at a constant rate, the glass fiber is exposed to the acid at different heights for different lengths of time. This results in a conical-formed taper. The taper angle θ can be determined by changing the speed v of the fluid level decrease according to the following formula

$$\theta = 2 \times \arctan \frac{c}{v} \tag{3.1}$$

where c is the HF etch rate. To prevent HF vapor from unintentionally attacking the fiber above the liquid, a protective film of silicon oil is applied over the HF. A typical etching process takes about 30 min. More details regarding the used HF concentrations, etch rates and flow rates can be found in [22].

3.4 Setup for coating a tapered fiber with SU8

After discussing how tapered fibers are fabricated, the coating of tapered fibers with SU8 is explained, which is a crucial step in experimentally verifying the possible coupling improvement. SU8 is a negative photoresist, so the procedure to coat a surface with that resist is similar compared to other photoresists. For this experiment SU8 3005 by microchem [43] is used. A schematic of the four fabrication steps to be performed are shown in Figure 3.3. First SU8 is applied to a target surface. After that, the applied SU8 has to be baked for some time, to evaporate solvents in the photoresist. Then, one has to expose the regions where one wishes the SU8 to stay, to light in the UV range from $\lambda \approx 350\,\text{nm} to 400\,\text{nm}$ [43]. After exposure, the resist needs to be developed. For SU8 the chemical 1-methoxy-2-propanol acetate $C_6H_{12}O_3$ is used. During the exposure step, the part of the SU8 that was not long enough exposed to UV light is removed and only the cured parts remain.

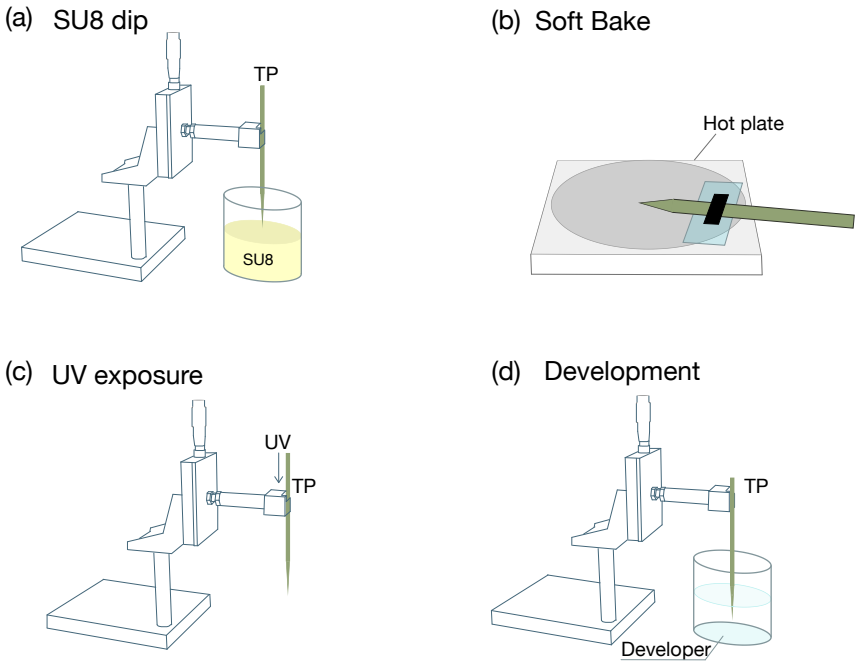

Figure 3.3: **Steps for coating tapered fiber with SU8**
This figure depicts the steps performed to coat tapered fibers with SU8, inspired by [1]. In step one (a) the fiber is dipped in SU8 3005. Step two (b) is the soft bake, where the fiber is taped on a glass plate on top of a hotplate in order to evaporate solvents in the photoresist. In step three (c) the coating is exposed to UV light from within the fiber. Several methods for coupling UV light into the fiber are tested for this thesis and are described in section 4.2. Step four (d) is to develop the coated fiber tip in SU8 developer.

For this coating procedure, the target surface in step one is the tip of the fiber and in step two the UV light exposure happens from within the fiber instead of curing from outside of the fiber. This ensures that all areas where light exits the tapered fiber tip are properly coated with cured SU8. For exposure two different light sources are tested, namely the Thorlabs M365FP1 UV LED, emitting light at 356 nm and the blue Thorlabs laser diode L405P150, emitting light at 405 nm. The coupling of UV light into the fiber was one of

the challenges of this thesis and is thoroughly explained in the result section 4.2. The times used for exposure are varied between 45 s and 8 min and the development times are varied between 30 s and 4 min. To make the dipping process reproducible, an optical fiber clamp (Thorlabs T711-250) was screwed to a manual linear stage (M-UMR5.25) with a micrometer screw (Newport BM11.25). With that tool, the dipping time could be held approximately constant where a typical example would be one screw turn every three seconds.

3.5 Coupling efficiency measurement setup

After having introduced the tapered fiber fabrication and the fiber coating procedure the question now remains how to measure if the SU8 coating method improved the coupling. For that, two steps are necessary. First, the coupling efficiency of the fiber has to be determined experimentally. After that the fiber is coated with SU8 and then the coupling efficiency with SU8 coating is measured again. To analyze the coupling efficiency, a chip with a silicon waveguide containing a photonic crystal mirror is used, as depicted in Figure 1.1. On a single chip usually many structures of the same design can be found, as can be seen in Figure 3.5. So in order to prove the improved coupling efficiency, the same fiber is coupled to five to ten different structures on the same chip before coating and then again after coating.

A schematic of the optical setup can be seen in Figure 3.4. The basic idea is to send light from a laser through a beam splitter. The first part of the light signal (excitation signal) is used as a reference signal to cancel out laser power fluctuations. That part is directly measured by a photodiode. The light signal in the other beam splitter arm is sent through the tapered fiber, coupled into the chip, reflected by the photonic crystal mirror in the silicon waveguide and then again measured by a photodiode (reflection signal). Through the ratio of excitation to reflection signal, the coupling efficiency can be measured. As a light source a Toptica CTL laser is used, which is tunable in the wavelength range from $\lambda = 1520\,\text{nm}$ to $\lambda = 1620\,\text{nm}$. The laser is connected to a free-space beam splitter setup (BS), using a single-mode fiber. A fiber collimation package (FC) is used, to couple the light into a free-space 50/50 beam splitter. The reason for using a free-space beam splitter and not a fiber-based beam splitter is to be able to adjust the polarization of the light with the help of a combination of a $\frac{\lambda}{2}$ and a $\frac{\lambda}{4}$-waveplate. This is needed to optimize the coupling efficiency into the waveguide. Also, the mirror reflectivity depends on the light polarization, so in order to get good coupling, it is helpful to be able to try different polarization to maximize the coupling. As described above, 50% of the laser power (the reflected part, called excitation signal P_e) is detected by a photodiode (Thorlabs PDA20CS2, PD1) and the other 50% (the transmitted part) is send to the tapered fiber, reflected by the waveguides' mirror and then again the power is measured by another photodiode (PD2) (called reflection signal P_r). The tapered fiber is held in place by a home-build fiber mount under an angle of 3°. Under the fiber tip the sample chip with the crystal cavity is installed and can be moved in the three space coordinates by a piezo stage (Thorlabs NanoMax300). A 0.5NA microscope objective (Thorlabs LMM-40X-P01, MO) is used to manually align the fiber with the waveguide. An LED brightens the image and the microscope image is transferred live to a computer with the help of a camera for visible light (VIS camera). An image taken with that camera of a successful coupling between a tapered fiber and a silicon waveguide on a typical PIC is shown in Figure 3.5.

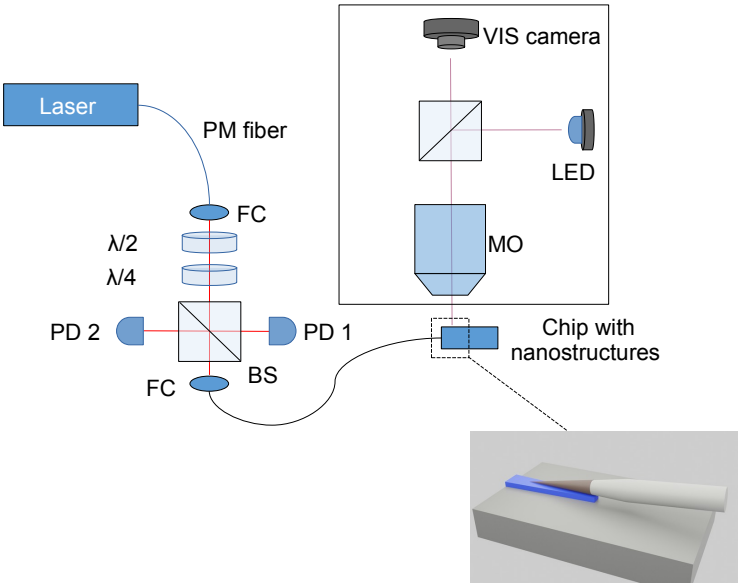

Figure 3.4: **Coupling efficiency measurement setup**
A Toptica CTL laser is coupled into a free-space beam splitter (BS) with a fiber collimation package (FC). The polarization of the incident light can be adjusted with the two $\frac{\lambda}{2}$ and a $\frac{\lambda}{4}$-waveplates. Two photodiodes (PD1 and PD2) are used to measure the excitation and reflection signal P_e and P_r. For coupling, the chip with the nanophotonic mirror has to be spatially aligned with the tapered fiber. To do that it can be optically observed with the help of a microscope objective (MO), an LED and a camera for visible light (VIS camera). Figure adapted from [44]

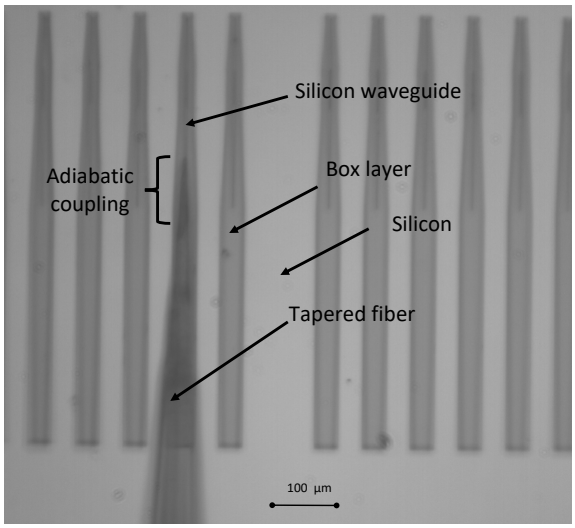

Figure 3.5: **Microscope image of successful adiabatic fiber-to-chip coupling**
A tapered fiber is aligned to a tapered silicon waveguide with the coupling efficiency measurement setup shown in Figure 3.4. The shown alignment leads to successful coupling. The BOx layer can be distinguished from the silicon by the difference in color. The image also shows that on a single chip typically many structures of the same design can be found.

3.5.1 Extracting the coupling efficiency

To calculate the coupling efficiency the reflection signal of the photonic crystal mirror in the waveguide is needed. Here, it is assumed that mirrors on the chip are perfect reflectors and that the propagation losses on the waveguide are negligible. Therefore, the calculated coupling efficiencies might be smaller than the actual values of the efficiencies.

In order to calculate the relative reflection signal rr, several transmission efficiencies have to be considered: The transmission efficiency of the beam splitter η_{bs}, the efficiency of focusing the transmitted beam (transmitted by the beam splitter) into the fiber η_{foc}, the coupling efficiency η_c and the collimation efficiency η_{col} which is the efficiency of coupling the from the chip reflected light back into the beam splitter and diode.

With that, rr can be calculated as [44]

$$rr = \frac{P_r}{P_e} = \eta_{bs}\eta_{col}\eta_c^2\eta_{foc} \tag{3.2}$$

.

An easy way to get η_c from this equation is to use a Faraday mirror (Thorlabs MFI-1550-APC), whose relative reflection can be calculated as

$$rr_{far} = \frac{P_r}{P_e} = \eta_{bs}\eta_{col}\eta_{far}\eta_{foc} \tag{3.3}$$

with η_{far} being the Faraday efficiency. The Faraday efficiency describes the ratio of incoming to reflected light for the Faraday mirror. η_{far} depends on the wavelength, for 1550 nm is is determined to be $\eta_{far} \approx 0.8$. Combining the above equations leads to:

$$\eta_c = \sqrt{\frac{rr}{rr_{far}}\eta_{far}} \tag{3.4}$$

So by measuring the relative reflection from the light leaving the waveguide, the coupling efficiency η_c can be measured.

Chapter 4

Results and discussion

In the previous chapter it was shown that SU8 coating of tapered fibers is a promising approach to improve the coupling efficiency in cryogenic packaging. In this chapter I want to investigate how the results described in [1] and the theory presented so far can be used to improve the exact fiber-to-chip coupling setup used by the "Quantum Networks group" at the MPQ. For this purpose the simulations conducted in [1] are adjusted to the waveguide geometry and materials used by the "Quantum Networks group". Additionally, I try to experimentally reproduce the tapered fiber coating steps described in [1] and investigate the coupling improvements with this method.

4.1 Simulation results

In order to adapt the simulation results described in [1] to the silicon waveguides used, the simulation setup described in 3.2 is used. Figure 4.1 shows the light intensity in the xz-plane cross-section of the simulation geometry. The tapered fiber points from right to left and the light source is positioned at $x \approx 65\,\text{cm}$ from where the light field is starting to travel towards the fiber tip and the silicon waveguide. What is interesting, is that the intensity is oscillating between fiber and waveguide over the whole taper region. The oscillation is observed with, as well as without the SU8 cap and even without BOx layer. Most probably this is due to an effect called cross-talk or mode beating between two waveguides. This is theoretically described and explained in [31] for example.

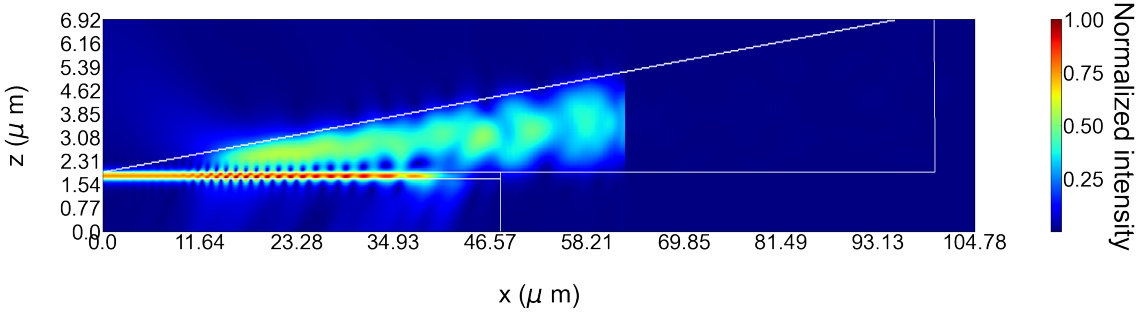

Figure 4.1: **Light intensity in cross-section of adiabatic coupling simulation**
The image depicts a xz-plane cross-section of the simulation geometry described in Figure 2.3. A light source on the right excites an eigenmode of the tapered fiber, which propagates to the left. The light is then coupled into the silicon waveguide on the left. The oscillations in light intensity can be explained by the phenomenon of cross-talk, also called mode beating, as described for example in [31].

The resulting coupling efficiencies, when the parameters overlap l, offset o and angle θ (as depicted in Figure 3.2) are swept across a range of values, are shown in Figure 4.2. I

find that the achieved coupling efficiencies do not reach the 90% reported in [1]. The most likely reason for that discrepancy are the SiN waveguides used in [1] instead of silicon waveguides. The refractive index of SiN waveguides ($n_{SiN} = 2.0$) is very different to that of silicon ($n_{Si} = 3.5$). $n_{SU8} = 1.55$ is a lot closer to n_{SiN} than to n_{Si}, which might lead to much better coupling. Because of this, other refractive index coatings are simulated later in this section to see if there are other materials better suited for silicon waveguides. But first, I want to discuss the results obtained from the parameter sweep using the SU8 coating.

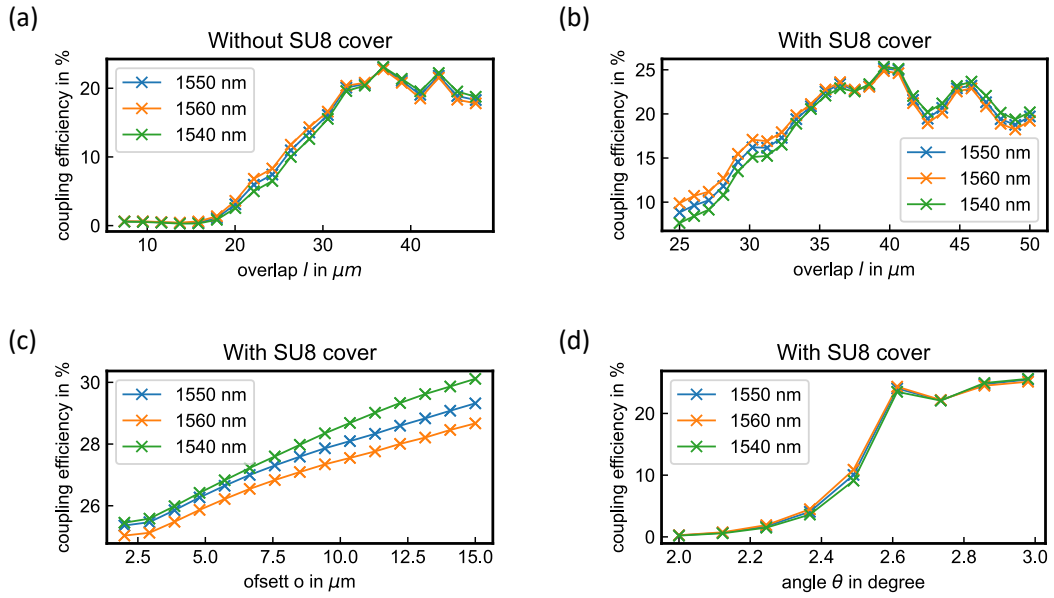

Figure 4.2: **Simulated coupling efficiency between an SU8-coated fiber and a waveguide as a function of four different sweep parameters**
Sweeping the parameters o, l and θ as shown in Figure 3.2 with the simulation geometry described in section 3.2. Panel (b), (c) and (d) show parameter space sweeps with an SU8 cap, Panel (a) shows an overlap sweep without the SU8 cap for reference. It can be seen that the larger the offset o and angle θ, the thicker the SU8 coating layer, the better the coupling efficiency. Coupling efficiencies near 90% with SU8 capped fibers as reported in [1] can not be replicated, most likely due to the different waveguide material (silicon instead of (SiN) as in [1]).

In Figure 4.2 (b) the coupling efficiencies are shown as a function of the fiber-to-waveguide overlap l for three different wavelengths centered around the middle of the telecom-C band using a realistic cap-offset of $o = 2\,\mu m$ and angle of $\theta = 2.98°$. The optimal overlap is around $l_{opt} = 40\,\mu m$ and achieves coupling efficiencies of about 25%. For reference, Figure 4.2 (a) shows the same parameter for a non-coated fiber. It can be seen, that the optimal overlap is slightly smaller with $l_{opt} = 37\,\mu m$. Additionally, a slightly smaller coupling efficiency of 23% is achieved.

Figures 4.2 (c) and (d) show the parameter sweeps of the offset o and coating angle θ. Although the coupling improvements are not as large as described in [1], the parameter sweep does show improvements. The result indicates, that the larger the angle θ, the better, with best coupling achieved at around $\theta = 2.98$. Increasing the offset o seems to linearly increase the coupling efficiency, leading to improvements of up to 10% compared to the reference simulation. The offset o is difficult to predict. It seems like realistic offsets

are in the range of 1 µm to 2 µm, where the coupling efficiency improvement is only around 3%. There, however, is a chance that the 10% coupling efficiency improvement is not as unrealistic, as the offset $o = 15\,\mu m$ might seem. This is because the geometry used might not be the most realistic approach. For example, instead of simulating the cap as a tapered cone, the cap could also be assumed to have a round tip for example. Using such a geometry could lead to the same coating thicknesses that lead to the 10% coupling improvements described above without the large offset at the tip.

In order to check if coatings with materials of higher refractive indices than SU8 lead to better results, as their refractive index would be closer to that of the silicon waveguide, further simulations are conducted, the results of which can be seen in Figure 4.3. The simulation geometry was again assumed to be as depicted in Figure 3.2 and the used parameters are offset $o = 2\,\mu m$, overlap $l = 40\,\mu m$ and angle $\theta = 2.98°$. The offset was selected in this way, as it represents a realistic cap thickness and the overlap l might not be the most optimal overlap in each case, however the tendencies of coupling efficiency should still be visible. As can be seen in Figure 4.3, coupling efficiencies of around 30% with refractive indices around $n = 2$ can be reached. However, these efficiencies are still nowhere near the reported 90% in [1]. For larger refractive indices, the coupling efficiency drops drastically. This is probably due to the fact, that the refractive index difference between fiber and SU8 coating is so large, that the concept of adiabatic coupling fails due to the large refractive index changes involved. Additionally, it can be seen in the simulation that for high refractive indices, the light is predominantly guided in modes restricted to solely the coating, which makes the concept of adiabatic coupling impossible. These issues could potentially be solved with a different coupling geometry. The investigation of this is left for further work.

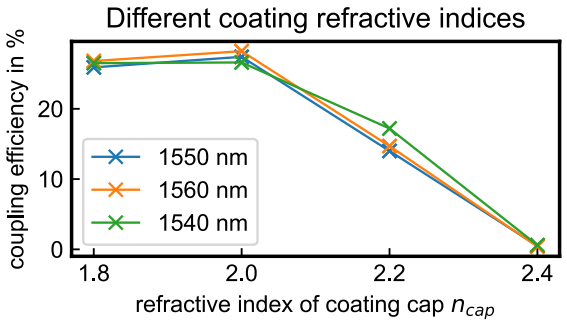

Figure 4.3: **Simulated coupling efficiency as a function of the refractive index of the coating**
Simulation results for different coating refractive indices with the geometry parameters $o = 2\,\mu m$, $l = 40\,\mu m$ and $\theta = 2.98°$, which is shown in Figure 3.2. The highest coupling efficiency is achieved with $n_{cap} = 2.0$, for a refractive index above $n_{cap} = 2.2$ the coupling efficiency drops drastically.

Table 4.1 summarizes the optimal coupling efficiencies found by sweeping the overlap l for the non-coated cases and the angle θ as well as the offset o for the SU8 coating. The parameters, for which the optimal coupling efficiency is observed are also given in the table.

Setup	Coupling efficiency [%]	Offset o [μm]	Optimal coupling parameters	
			Overlap [μm]	θ [°]
without BOx	95	-	34	-
with BOx	22.8	-	37	-
with BOx & SU8	25	2	40	2.98
with BOx & SU8	30	15	40	2.98

Table 4.1: **Summary of results from different simulation scenarios**
Summary of parameter values and corresponding optimal coupling efficiencies for different simulation scenarios. Coupling without BOx layer achieves the highest efficiencies. Coupling with BOx layer achieves better results when using SU8 coating.

4.2 Fabricating SU8 coating

The simulation results described in section 4.1 promise coupling improvements up to 10%, depending on how thick the SU8 coating can be experimentally realized. The coupling improvement potential together with all the benefits described in chapter 3.1 compared to other coating mechanisms, make the experimental realization of SU8 coating worth a try. For investigating the coating of tapered fibers with SU8, three experimental intermediate steps are performed. The first step is finding a way to reliably detect if a tapered fiber is coated with SU8. Secondly, different UV exposure methods are investigated and as a third step after successfully coating tapered fibers, their coupling efficiencies before and after coating are compared.

4.2.1 Determining if a fiber was successfully coated

A very important step for comparing SU8 coating methods is to be able to tell whether a fiber is coated or not. Measuring the coupling efficiency for the fiber before and after coating with the optical setup described in 3.5 is one possible approach. The problem here is, that the simulations are not very clear regarding a measurable coupling improvement. Also, coupling itself is very time consuming and sensitive to a lot of parameters, so it has to be performed several times to get a good idea about the best possible coupling efficiency. So, it would be more efficient to first optically check the coating results before measuring the coupling itself. The question is if the SU8 coating is optically visible using a microscope. In [1] the authors are able to see SU8 coated tapered fiber tips under a standard optical microscope. To get a better sense on how a coated glass surface looks like in a microscope image, coating a microscope glass slide with SU8 was attempted, because it is a lot easier to coat than tapered fibers. Therefore, the SU8 is carefully spread on the glass plate with a pipette and then irradiated with the UV LED. The coated regions were clearly visible under the microscope by the visible smears at their edges which most likely result from interference phenomena (Figure 4.4). Although the SU8 layer thickness is probably a lot larger on the glass slide than on the fiber, the two observations are strong evidence that at least something should be visible when a fiber is coated with SU8.

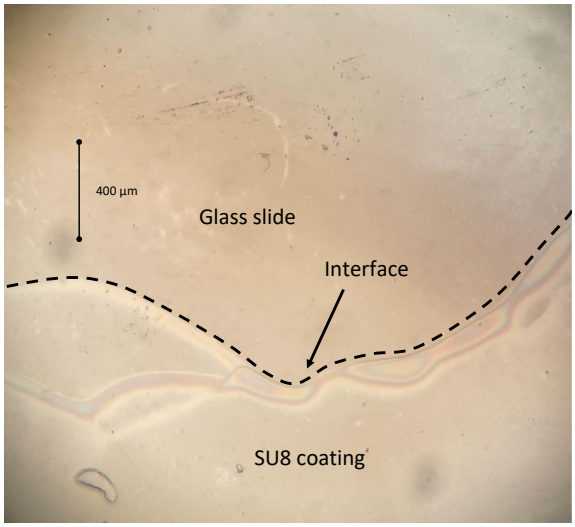

Figure 4.4: **SU8 coated glass slide**
Glass slide under an optical microscope coated with SU8 to get a feeling for how SU8 coating layers look like. The SU8 is clearly identifiable at the SU8 layer edge by the visible interference patterns.

4.2.2 UV exposure methods

A critical step in the SU8 coating procedure is the UV exposure step. If no or too little UV light reaches the fiber tip, all SU8 will be removed during the development step. Because of this, different UV exposure methods are tested, all of them having their own advantages and disadvantages. Figure 4.5 shows sketches of the different exposure methods.

One possible light source for UV exposure is the M365FP1 Thorlabs UV LED also mentioned in section 3.4. This method is inspired by [1]. The LED has the great advantage of being portable, so the UV exposure can happen in the same laboratory where the SU8 dipping and development steps are performed. Additionally, no expensive laser setup is needed. The problem with the LED is, that its output is optimized for multi-mode fibers. However, the UV light has to be coupled into the single-mode tapered fiber at some point. There are three possibilities for coupling the UV light from the LED into the single-mode fiber with the tapered end, one free-space method and two fiber coupling methods. The fiber coupling methods are depicted in Figure 4.5 (a) and (d). In method (a) a single-mode SMA adapter (Thorlabs P2-SMF28-PCSMA-1, depicted as C1 in Figure (a)) is used to directly couple the UV light into the single-mode tapered fiber. In method (d) on the other hand, a multi-mode SMA adapter (Thorlabs M131L01, depicted as C2 in (d)) is used to first couple the UV light into a multi-mode fiber and then coupling the light from the multi-mode to the single-mode fiber using a mating sleeve, depicted as C in (d). As the first approach depicted in (a) requires only one coupling interface, this method is tried first, since interfaces always cause losses. Method (d) was not tried and is left for a future work. Method (a) failed, because too little light arrived at the fiber tip. After the patch cable, maximally 10 nW of the initial 15.5 mW are measurable, so almost all light is lost at the interface between LED and SMA adapter. This would still be enough for a successful exposure. However, behind the patch cable a splice for coupling into the tapered fiber is necessary. The splice, together with the fact that the single-mode fibers used are not optimized for transmitting UV light lead to further significant losses. As it is very difficult to accurately measure the amount of light exiting the tapered fiber tip, coating is attempted in a few cases to see if the intensity reaching the tip is sufficient. The

experiments show, that this is not the case. Table 4.2 shows a few example data of the failed attempts. The fibers are all named starting with a capital R and then chronologically numbered.

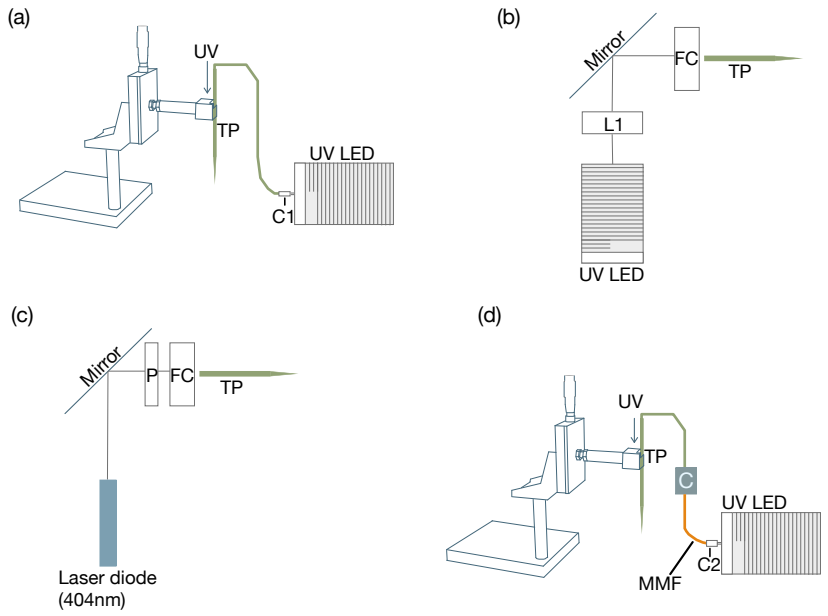

Figure 4.5: **UV exposure methods**
As the UV exposure step is critical for successful coating, several different methods are tested. Figure (a), (b) and (d) depict three possibilities of coupling light from a UV LED into the tapered fiber. Methods (a) and (b) were tested and did not lead to enough UV light reaching the fiber tip. Method (c) shows a successful exposure method, in which a blue laser diode is free-space coupled into the tapered fiber. Method (d) uses a multi-mode fiber in between the UV LED and the tapered fiber. The advantages here are discussed in the text.

Fiber Name	Exposure Time	Development Time	Dipping Speed	Conclusion
R11	60 s	2 min	one turn in three seconds	tip was destroyed during coating process, see figure 4.6 (a)
R22	4 min	2 min	one turn in three seconds	no coating
R23	45 s	2 min	one turn in three seconds	no coating, see Figure 4.6 (b)

Table 4.2: **Example coating parameters of unsuccessful coating attempts with UV exposure method (a)**
The table shows the coating parameters used for a few exemplary attempts of coating tapered fibers with SU8 using UV exposure method (a), shown in Figure 4.5. As the conclusion column indicates, all of the coating attempts failed.

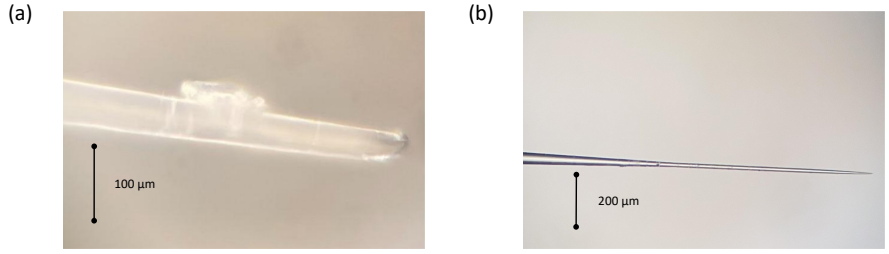

Figure 4.6: **Failed coating attempts with UV exposure method (a)**
Figure (a) shows fiber R11 after coating. The tapered fiber tip was destroyed during the coating process and no SU8 cap can be seen. Figure (b) shows fiber R22 after attempted coating, which survived but is not coated. Details about the coating parameters used for the fibers are shown in table 4.2. For both fibers UV exposure method (a) from Figure 4.5 was used, meaning that the UV LED was coupled with a single-mode SMA adapter into the tapered fiber.

Another method to couple the LED output to single-mode fibers is to use free-space coupling. This is done by collimating light emitted by the UV LED with a lens ($f = 25\,\text{mm}$, L1 in 4.5 (b)) and coupling the collimated beam over a mirror (Thorlabs PF 10-03-P01) into a single-mode fiber using a fiber collimator (FC) (Thorlabs TC18FC-405). This method also failed as no detectable signal arrived after the fiber collimator. A possible reason might be the large angles at which light is exiting the LED such that it cannot be efficiently focused by the lens. Additionally, the mirror used is optimized for wavelengths of above 450 nm, so some losses might occur here. With a power meter, however, it was measured that after the mirror at least 30% of the light was still arriving at the fiber collimator, so the most probable reason for getting no measurable signal at all is the fiber collimator. The collimator at hand is optimized for 405 nm light and not 365 nm, meaning that probably almost all the losses occurred there.

Another available light source for UV exposure is a blue laser diode (Thorlabs L405P150). As the laser diode emits an elliptical beam, the beam has to be transformed into a circular beam for the fiber collimator (FC) by using an anamorphic prism pair, depicted as P in Figure 4.5 (c). The blue diode has the advantage of being able to produce light powers up to 150 mW in a collimated beam, making it very easy to couple the light free-space into a single-mode fiber, leading to intensities of the order of 10 mW in the fiber. There are two problems here: First, the diode is emitting at 405 nm. No information is found about how this influences exposure times in the data sheet of the SU8. This is why for this method very long exposure times between 6 min and 12 min are chosen. Second, the blue diode is permanently installed in a different laboratory, such that the freshly dipped tapered fiber has to be moved between different laboratories. This makes reproducibility suffer and the probability of a lot of fibers breaking during the process is increased dramatically. Despite these two problems, it was possible to coat two tapered fibers (R26 and R33) with this method. Pictures of both fibers before (R26 (a), R33 (c)) and after coating (R26 (b), R33 (d) and (e)) are shown in Figure 4.7. The Figures 4.7 (d) and (e) both show R33 after successful coating but with different microscope objectives. The coating parameters used are documented in table 4.3. As can be seen in the table, R33 was only successfully coated on the second attempt. Why the first attempt failed is not known. The only parameter varied is the dipping speed. However for the first fiber, the slow dipping speed lead to successful coating, so there probably is another reason involved.

Fiber Name	Exposure Time	Development Time	Dipping Speed	Conclusion
R26	6 min	2 min	one turn in three seconds	coating visible, see Figure 4.7 (b)
R33 first attempt	6 min	2 min	one turn in three seconds	no coating visible
R33 second attempt	4 min	2 min	one turn in one second	coating visible, see Figure 4.7 (d) and (e)

Table 4.3: **Coating parameters of successful coating attempts with UV exposure method (e)**
Parameters used for the two successful coating attempts using UV exposure method (e) shown in Figure 4.5. The table shows that fiber R33 was only successfully coated on the second attempt for unknown reasons.

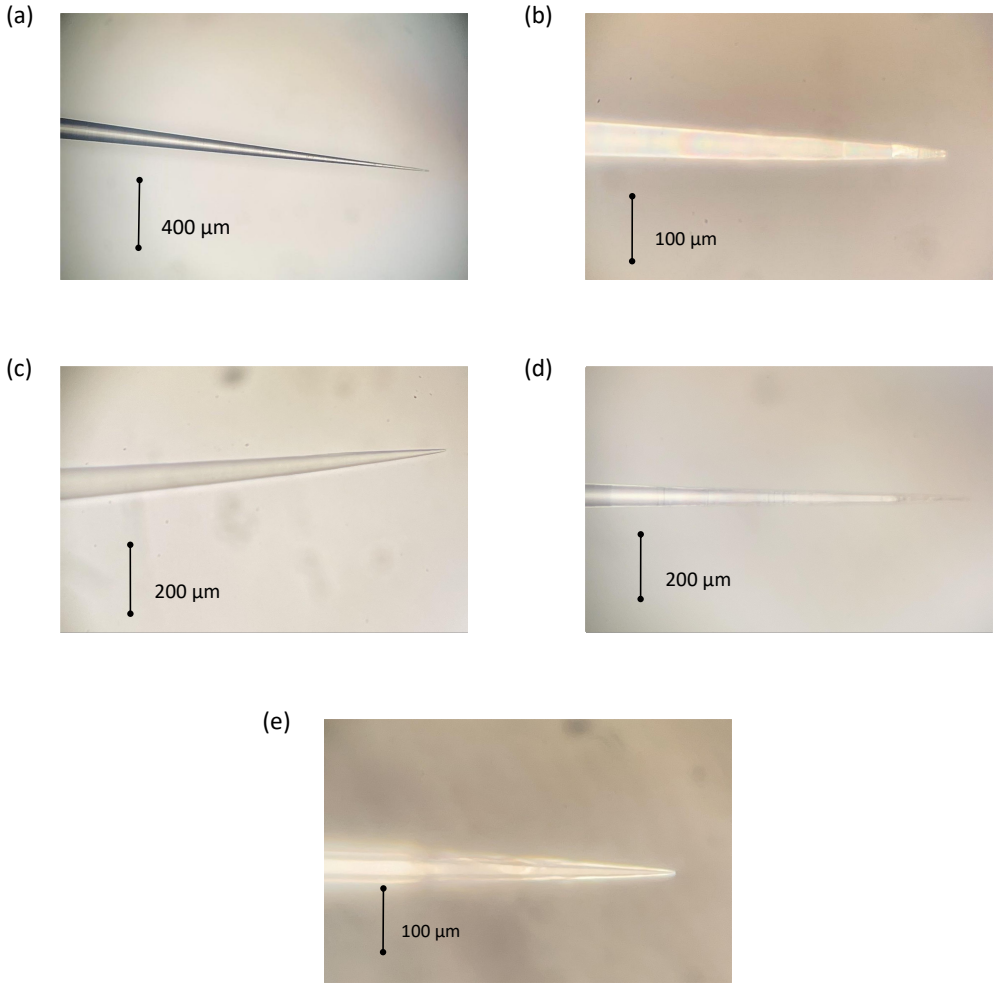

Figure 4.7: **Successful coating attempts with UV exposure method (c)**
Image (a) and (b) depict fiber R26 before and after coating. Image (c) depicts fiber R33 before coating and (d) and (e) both depict fiber R33 after the successful coating attempt with different magnifications. Details about the coating parameters used for the fibers are shown in table 4.3. Images (b), (d) and (e) show the typical smears observed for SU8 coating layers, as shown in Figure 4.4. Image (e) shows a close up of the R33 fiber tip, showing irregularities in the SU8 coating.

4.3 Coupling efficiency measurements using capped tapered fibers

After successfully finding a way of coating tapered fibers, it is now possible to measure their coupling efficiency before and after the coating. As the optical coupling depends on exact alignment, polarization and cleanliness of fiber, in order to reliably detect a coupling improvement, the coupling has to be tested on multiple waveguide structures (in this work around five to ten), before and after the coating. Of these measurements the best coupling achieved is assumed to be the maximum possible coupling. The results for the two fibers where an SU8 coating was visible can be seen in table 4.4. The details of the fabrication of their coating are given in table 4.3. Unfortunately, the results for the first coated fiber (R26) are inconclusive, as the coupling before the coating was very low with 4.2%. However, after coating the fiber, very good coupling results of 18.9% were achieved. It is unlikely, that this big of an improvement is only due to the SU8. It is more probable that an error occurred during the first coupling without the coating which is mistaken for a fabrication issue. Possible reasons include improper adjustment of the polarization of the incoming laser light as well as a bad splice. Nevertheless, the result is useful, as it shows that coupling with coated fibers is indeed possible and can lead to good coupling results. The second coated fiber showed significantly worse coupling after the coating (4%) than before coating (15.2%). This is not a big surprise as the coating is very non-uniform, as can be seen in Figure 4.7 (d) and (e), so probably a lot of light is scattered at the fiber tip. A possible reason for the non-uniformity is the fast dipping speed, as also described in [1]. A detailed investigation of this is left for future work.

Fiber Name	**Coating Method**	**Maximum Coupling Efficiency**	
		before	after
R26	method 3	4.2%	18.9%
R33	method 3	15.2%	4.0%

Table 4.4: **Measured maximum coupling efficiencies from successfully coated tapered fibers**
The table shows the results from measuring the coupling efficiencies of the successfully coated fibers R26 and R33 before and after SU8 coating with UV exposure method (c). The maximum coupling efficiency is determined by measuring the coupling efficiency on multiple different waveguide structures and taking the maximum achieved coupling value.

4.4 Determining SU8 layer thickness on cleaved fibers

Very crucial parameters are the thickness and shape of the SU8 coating layer. By precisely knowing these numbers, the simulations could be made more accurate and better predictions about coupling improvements would be possible. There are several tools available for investigating the SU8 layer, like for example white light interferometry, atomic force microscopy or scanning electron microscopy. Here I use a white light interferometer (WLI) as it is available in a neighboring laboratory and easy to use. With that device it is a lot easier to investigate the cross-section of cleaved fibers than a tapered fiber tip, as the rounding of the tapered fibers make it very difficult to obtain a reliable surface profile. Although the coating structure of tapered fibers is most likely very different to cleaved fibers, the coating layer thickness on cleaved fibers might still give a first idea of the possible thickness scale. The coating process used for the cleaved fiber is the same as for the tapered fibers, using

the working UV exposure method with the blue LED described in section 4.2. An exposure time of 6 min is selected and 2 min development times are chosen, since these were the times used for the coated tapered fibers. The surface structure of the cleaved fibers is measured using the WLI before and after coating. The results can be seen in Figure 4.8. Figure 4.8 (a) and (b) show the surface profile before coating, Figure (c) and (d) the profile after coating. It is clearly visible that around the fiber center a 40 µm high and 35 µm wide bulge can be seen. The slope of that bulge is too steep for the white light interferometer to resolve, which is why the profile is not visible at some points. That bulge is located above the core, so exactly where the UV light exits the fiber and is able to harden the photoresist. The results from this experiment show, that coating thicknesses can be quite thick and although the coating structure of a tapered fiber probably looks very different, it indicates that thicknesses of 10 µm could possibly be fabricated with tapered fibers and coupling improvements of around 10% might actually be achieved. The coating procedure and measurements with the cleaved fibers turned out to be very easy and reproducible, as they are mechanically a lot more stable than tapered fibers and their surface profile is easily analyzable. So using this method in further work might be a great method of investigating the effects of changes in exposure and development times and also to test new UV exposure method, like for example the proposed method for future work shown in Figure 4.5 (d).

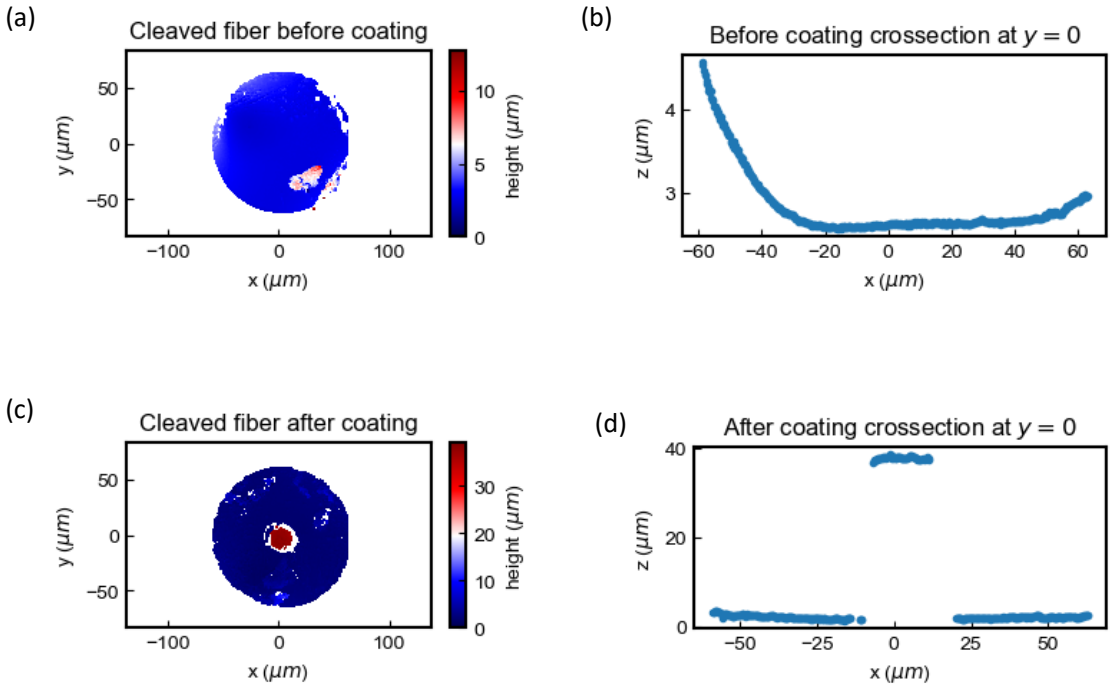

Figure 4.8: **Surface structure of cleaved fiber before and after SU8 coating**
The plots show surface structure data taken with a white light interferometer. Figure (a) and (b) show the height profile and surface cross-section of a cleaved fiber before SU8 coating respectively. The cross-section shows a maximum height difference of around 4 µm. Figure (c) and (d) show the same data for the cleaved fiber after SU8 coating with the same procedure as explained for the tapered fibers using exposure method (c). A clear 40 µm high and 35 µm wide bulge can be seen around the fiber core.

4.5 Additional simulation towards cryogenic packaging

So far, this thesis focused on improving coupling between on-chip waveguides and optical fibers by coating tapered fibers with higher index materials, as this method would be a good compromise between ease of fabrication, broadband transmission and coupling efficiency. However, improving coupling efficiency is not the only issue in cryogenic packaging. As mentioned already in the introduction, coupling in cryostats is difficult, since expensive cryogenic positioners are needed. Such positioners require additional cooling power, a lot of space (which is often not present in cryostats) and an optical access, complicating the overall cryogenic setup. Therefore, it is preferred to align the tapered fiber with the waveguide outside of the cryostat and then fix their position, by for example gluing the fiber onto the waveguide. This method is currently used for cleaved single-mode fibers with the glue Norland Optical Adhesive 88 ($n = 1.56$). This glue has a low refractive index and still good mechanical properties at cryogenic temperatures below 2 K. For uncoated tapered fibers this method is not applicable, as the refractive index of the fiber cladding $n_{cl} = 1.457$ is smaller than that of the glue, so that no total reflection between the light in the fiber and the glue surrounding the fiber happens anymore, leading to almost all light being lost. Coating tapered fibers could present a way, how they could anyway be glued onto a waveguide. This is what I investigate in the following two simulations, by checking which refractive index for the adhesive are made possible by the SU8 coating.

As the refractive index of SU8 is larger than that of the glass fiber, the question is which refractive index the glue needs to have in order to be a suitable choice. Figure 4.9 shows a parameter sweep of an SU8 coated fiber with the exact same geometry as discussed in chapter 4.1, where the background refractive index is swept between $n = 1.0$ and $n = 1.6$, which represents the glue that encases the whole system. It can be seen that up to a refractive index of $n = 1.4$ the achieved coupling results are similar to the previously obtained ones. However, above that threshold, no coupling is possible as the coupling efficiency decreases to zero. So in order to glue SU8 coated fibers onto a chip, an adhesive with $n \leq 1.4$ would have to be found.

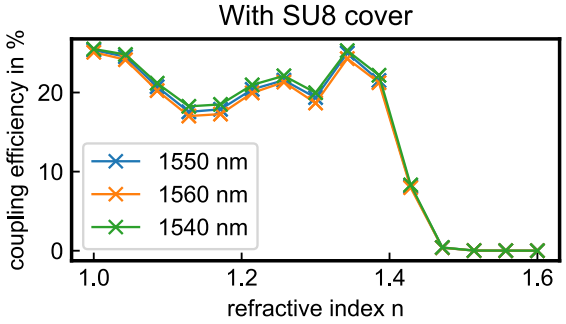

Figure 4.9: **Sweeping background refractive index for SU8 coating simulation**
Result of sweeping the background refractive index of an adiabatic coupling with an SU8 coated tapered fiber using offset $o = 2\,\mu m$, angle $\theta = 2.95°$ and overlap $l = 40\,\mu m$ for the parameters depicted in Figure 3.2. It can be seen, that for refractive indices above $n > 1.4$ the coupling decreases drastically.

Chapter 5

Summary and outlook

In this thesis I investigated a novel approach for improving cryogenic packaging by coating adiabatic tapered fibers with the photoresist SU8 as described in [1]. This method would represent a great compromise between broadband transmission, mechanical stability, ease of fabrication and coupling efficiency. As the authors in [1] investigate coupling to SiN waveguides and the "Quantum Networks group" uses silicon waveguides on their chips, I adapted the experiments described in that paper to the coupling setup used by the group here. To do so, I first simulated the coupling to the silicon waveguides with SU8 coated tapered fibers and varied several parameters. The simulations showed, that indeed coating the fiber with SU8 leads to larger coupling efficiencies. Generally speaking, the thicker the SU8 coating, the higher the efficiency. Thick coatings can achieve improvements of up to 10%, however these coatings are unreasonably thick especially at the fiber tip. Realistic SU8 layer thicknesses of below 2 µm lead to coupling efficiencies of around 25%. This however represents only a 3% improvement compared to non-coated fibers. The authors of [1] obtained simulated coupling efficiencies over 90%. The most likely reason for the discrepancy between their simulation and the simulations conducted in this thesis, is the large refractive index difference between silicon and SU8 compared to the difference between SiN and SU8. Simulating higher refractive indices than n_{SU8} for the coating cap did not lead to significantly better results and requires further investigation.

After showing that according to the simulations coupling improvements are expected, coating fiber tips with SU8 was attempted. Therefore, three experimental intermediate steps were achieved. First, it was shown that SU8 coated surfaces are visible using a standard optical microscope. After that, three different UV exposure methods were tested. The most promising was using a strong blue laser diode for free-space coupling into the single-mode fiber. With that method it was possible to coat tapered fibers with SU8. Having found a working coating method, the coupling efficiencies of the fibers before and after SU8 coating were measured. These measurements showed, that good coupling with SU8 coated fibers is possible, however it was not yet possible to see coupling improvements, most likely because of non-uniform SU8 coatings due to the dipping process. To additionally get an idea of the SU8 layer thickness, cleaved fibers were coated using the same method as for the tapered fibers. Measurements using a white light interferometer indicated layer thicknesses above 35 µm for cleaved fibers, making a layer thickness of 10 µm at the tapered fiber tip more realistic. This indicated that maybe coupling improvements of 10% would be possible.

Cryogenic packaging requires not only good solutions for high coupling efficiencies but also for solving the problem of the difficulty of coupling within cryostats. Coating tapered fibers with a high index material would allow for gluing them onto waveguides. To further investigate this approach, further simulations of tapered fibers coated with SU8 were conducted, to estimate the maximum allowed refractive index. For SU8, in order to get coupling efficiencies above 15% a glue with a refractive index below $n \leq 1.4$ is needed,

which, unfortunately, is not available right now.

To summarize, this thesis showed that coating tapered fibers with SU8 could lead to coupling improvements for fiber-to-chip coupling with silicon waveguides, depending on the achievable SU8 coating thicknesses. A working coating method was found, however, coupling improvement with the coated fibers was not yet achieved. In future work the coating method has to be optimized, to lead to uniform SU8 coatings with little light scattering. One idea making the coating procedure more reproducible would be to find a coating method that does not require to change laboratories during fabrication. To achieve this, the presented method of coupling the used UV LED into a multi-mode cable and then coupling the light from the multi-mode cable into a single-mode cable could be tried. For testing new UV exposure methods, coating cleaved fibers instead of tapered fibers might be a way of speeding up the testing process.

Bibliography

[1] Saeed Khan et al. »Low-loss, high-bandwidth fiber-to-chip coupling using capped adiabatic tapered fibers«. In: *APL Photonics* 5.5 (1st May 2020). Publisher: American Institute of Physics, p. 056101. DOI: 10.1063/1.5145105.

[2] R.G. Hunsperger. *Integrated Optics: Theory and Technology*. Advanced texts in physics. Springer New York, 2009.

[3] R. Osgood and X. Meng. *Principles of Photonic Integrated Circuits: Materials, Device Physics, Guided Wave Design*. Graduate Texts in Physics. Springer International Publishing, 2021.

[4] A. McGurn. *Nanophotonics*. Springer Series in Optical Sciences. Springer International Publishing, 2018.

[5] S.V. Gaponenko. *Introduction to Nanophotonics*. Introduction to Nanophotonics. Cambridge University Press, 2010.

[6] H. Benisty, J.J. Greffet and P. Lalanne. *Introduction to Nanophotonics*. Oxford Graduate Texts. Oxford University Press, 2022.

[7] Weiwei Zhang et al. »Silicon nanobeam cavity for ultra-localized light-matter interaction«. In: *Opt. Lett.* 42.17 (Sept. 2017). Publisher: Optica Publishing Group, pp. 3323–3326. DOI: 10.1364/OL.42.003323.

[8] Mohamed A. Swillam et al. »On Chip Optical Modulator using Epsilon-Near-Zero Hybrid Plasmonic Platform«. In: *Scientific Reports* 9.1 (30th Apr. 2019), p. 6669. DOI: 10.1038/s41598-019-42675-z.

[9] Seung-Woo Jeon et al. »Diamond photonic crystal mirror with a partial bandgap by two 2D photonic crystal layers«. In: *Opt. Express* 28.26 (Dec. 2020). Publisher: Optica Publishing Group, pp. 39048–39057. DOI: 10.1364/OE.413172.

[10] Andreas Reiserer and Gerhard Rempe. »Cavity-based quantum networks with single atoms and optical photons«. In: *Rev. Mod. Phys.* 87.4 (Dec. 2015). Publisher: American Physical Society, pp. 1379–1418. DOI: 10.1103/RevModPhys.87.1379.

[11] David D. Awschalom et al. »Quantum Spintronics: Engineering and Manipulating Atom-Like Spins in Semiconductors«. In: *Science* 339.6124 (2013), pp. 1174–1179. DOI: 10.1126/science.1231364.

[12] P. Kómár et al. »A quantum network of clocks«. In: *Nature Physics* 10.8 (1st Aug. 2014), pp. 582–587. DOI: 10.1038/nphys3000.

[13] Stephanie Wehner, David Elkouss and Ronald Hanson. »Quantum internet: A vision for the road ahead«. In: *Science* 362.6412 (2018). DOI: 10.1126/science.aam9288.

[14] Lorenz Weiss et al. »Erbium dopants in nanophotonic silicon waveguides«. In: *Optica* 8.1 (Jan. 2021). Publisher: Optica Publishing Group, pp. 40–41. DOI: 10.1364/OPTICA.413330.

[15] Andreas Gritsch et al. *Narrow optical transitions in erbium-implanted silicon waveguides*. Issue: arXiv:2108.05120. 11th Aug. 2021.

[16] L. Vivien and L. Pavesi. *Handbook of Silicon Photonics*. Series in Optics and Optoelectronics. CRC Press, 2016.

[17] C. Yeh and F. Shimabukuro. *The Essence of Dielectric Waveguides*. Springer US, 2008.

[18] Bucholtz Singley. *A Brief Introduction to Core Modes in Optical Fiber*. 2021.

[19] J.D. Jackson. *Classical Electrodynamics*. Wiley, 2012.

[20] Steven G. Johnson and J. D. Joannopoulos. »Block-iterative frequency-domain methods for Maxwell's equations in a planewave basis«. In: *Opt. Express* 8.3 (Jan. 2001). Publisher: Optica Publishing Group, pp. 173–190. DOI: 10.1364/OE.8.000173.

[21] J. E. Goell. »Rectangular Dielectric Waveguides«. In: *Introduction to Integrated Optics*. Ed. by Michael K. Barnoski. Boston, MA: Springer US, 1974, pp. 73–103. DOI: 10.1007/978-1-4684-2082-1_4.

[22] Lorenz Weiß. »Erbium dopants in silicon nanophotonic waveguides«. PhD thesis. Technische Universität München, 2022.

[23] M. Azadeh. *Fiber Optics Engineering*. Optical Networks. Springer US, 2009.

[24] Miodrag Scepanovic et al. »Design and Processing of High-Density Single-Mode Fiber Arrays for Imaging and Parallel Interferometer Applications«. In: *Applied optics* 43 (Aug. 2004), pp. 4150–6. DOI: 10.1364/AO.43.004150.

[25] J.A. Stratton. *Electromagnetic Theory*. IEEE Press Series on Electromagnetic Wave Theory. Wiley, 2007.

[26] E. Snitzer. »Cylindrical Dielectric Waveguide Modes$\ast$«. In: *J. Opt. Soc. Am.* 51.5 (May 1961). Publisher: Optica Publishing Group, pp. 491–498. DOI: 10.1364/JOSA.51.000491.

[27] D. Gloge. »Weakly Guiding Fibers«. In: *Appl. Opt.* 10.10 (Oct. 1971). Publisher: Optica Publishing Group, pp. 2252–2258. DOI: 10.1364/AO.10.002252.

[28] Xin Mu et al. »Edge Couplers in Silicon Photonic Integrated Circuits: A Review«. In: *Applied Sciences* 10.4 (2020). DOI: 10.3390/app10041538.

[29] B. Chen et al. »Two-dimensional grating coupler on silicon with a high coupling efficiency and a low polarization-dependent loss«. In: *Opt. Express* 28.3 (Feb. 2020). Publisher: Optica Publishing Group, pp. 4001–4009. DOI: 10.1364/OE.380338.

[30] Riccardo Marchetti et al. »Coupling strategies for silicon photonics integrated chips«. In: *Photon. Res.* 7.2 (Feb. 2019). Publisher: Optica Publishing Group, pp. 201–239. DOI: 10.1364/PRJ.7.000201.

[31] A.W. Snyder and J. Love. *Optical Waveguide Theory*. Science paperbacks. Springer, 1983.

[32] T. G. Tiecke et al. »Efficient fiber-optical interface for nanophotonic devices«. In: *Optica* 2.2 (Feb. 2015). Publisher: Optica Publishing Group, pp. 70–75. DOI: 10.1364/OPTICA.2.000070.

[33] J. D. Love et al. »Tapered single-mode fibres and devices. Part 1: Adiabaticity criteria«. In: *IEE Proceedings J (Optoelectronics)* 138.5 (Oct. 1991), 343–354(11).

[34] D.B. Davidson. *Computational Electromagnetics for RF and Microwave Engineering*. Cambridge University Press, 2010.

[35] John Schneider. *Understanding the FDTD Method*. Section: 3.

[36] A. Neubauer. *DFT - Diskrete Fourier-Transformation: Elementare Einführung*. Vieweg+Teubner Verlag, 2012.

[37] J.P. Bérenger. *Perfectly Matched Layer (PML) for Computational Electromagnetics*. Synthesis lectures on computational electromagnetics. Morgan & Claypool Publishers, 2007.

[38] *Lumerical*. FDTD.

[39] A. M. Dibos et al. »Atomic Source of Single Photons in the Telecom Band«. In: *Phys. Rev. Lett.* 120.24 (June 2018). Publisher: American Physical Society, p. 243601. DOI: 10.1103/PhysRevLett.120.243601.

[40] T. G. Tiecke et al. »Efficient fiber-optical interface for nanophotonic devices«. In: *Optica* 2.2 (Feb. 2015). Publisher: Optica Publishing Group, pp. 70–75. DOI: 10.1364/OPTICA.2.000070.

[41] Michael J. Burek et al. »Fiber-Coupled Diamond Quantum Nanophotonic Interface«. In: *Phys. Rev. Applied* 8.2 (Aug. 2017). Publisher: American Physical Society, p. 024026. DOI: 10.1103/PhysRevApplied.8.024026.

[42] Hamed Nikbakht et al. »Fabrication of Tapered Tip Fibers With a Controllable Cone Angle Using Dynamical Etching«. In: *J. Lightwave Technol.* 33.23 (Dec. 2015). Publisher: Optica Publishing Group, pp. 4707–4711.

[43] KAYAKU microchem. *SU-8 3000 Permanent Epoxy Negative Photoresist*.

[44] Johannes Früh. »Optimization of the coupling to photonic crystal resonators«. master thesis. Department of Applied Sciences and Mechatronics: University of Applied Sciences Munich.

Acknowledgements

This thesis was only possible with the great support from many people. I especially want to thank:

- Prof. Dr. A. Reiserer for giving me this highly interesting thesis topic that helped me to learn a great deal about experimental research and simulations. I additionally want to thank him for his great support throughout this thesis by always having time for my questions and extensive result discussions. His ideas were extremely valuable I learned a lot from them. Lastly I want to thank him for prove-reading my thesis so thoroughly and his valuable feedback.
- Dr. L. Weiss for the incredible effort and patience he put into prove-reading my thesis and for also answering all my questions without ever being annoyed.
- Stephan Rinner for always answering all of my questions, helping me with my experimental setups, prove-reading my thesis and always having time for me when I needed help.
- Florian Burger for helping me with the experimental setups, discussing questions and prove-reading my thesis.
- Johannes Früh for helping me with all the optical setups and microscopes and answering tons of questions without being fed-up.
- Andreas Gritsch for greatly supporting me with the simulations.
- Nilesh Goel for having so much patience with explaining the RT setup to me and debugging it and also for staying up very late at night just to help me with my measurements.
- The whole "Quantum Networks group" in general for being so open, supportive and everyone always being accessible for questions and discussions.
- My family and my friends (especially my mum, my sister Chiara, and friends Clara, Salome, Dominik and Yordan) for mentally encouraging and supporting me and dealing with my moods when again nothing worked and I was frustrated.
- Felix Schwarzfischer for his mental support and the endless valuable discussions about the theory behind waveguides and fiber-to-chip coupling.